Archives of Acoustics Vol. 47, No. 1, pp. 25–31 (2022), doi: 10.24425/aoa.2022.140729

Research Paper

Perfect Absorption for Modulus-Near-Zero Acoustic Metamaterial in Air or Underwater at Low-Frequency

Fatma Nafaa GAAFER

Department of Science, College of Basic Education, Wasit University
Iraq; e-mail: fnafie@uowasit.edu.iq

(*received March 31, 2021; accepted November 13, 2021*)

We theoretically propose a method to achieve an optimum absorbing material through a modulus-near-zero (MNZ) metamaterial immersed in air or water with a change in slit width part. The destructive interference has paved the way to achieve perfect absorption (PA). Depending upon theoretical analysis, an acoustic metamaterial (AMMs) that supports resonance with a monopole (140 Hz) is developed to construct a low-frequency sound-absorbing technology. The dissipative loss effect can be by attentively controlling onto slit width to achieve perfect absorption. When there are thin slit width and visco-thermal losses in the structure, it is observed that they lead to high absorption. We use finite element simulations via COMSOL Multiphysics software to theoretical measurement in impedance tube and show the influence of structural parameters in both mediums. The results are of extraordinary correspondence at low frequency to achieve optimum perfect absorption (99%). That might support AMMs to actual engineering-related applications in the process of mitigating noise, slow sound trapping, notch filtering, energy conversion, and time reversal technology.

Keywords: acoustic metamaterial; perfect absorption; Fabry-Pérot resonances; subwavelength scale; modulus-near-zero.

1. Introduction

Recent years have seen the appearance of two types of structures for wave modulation, known as metasurfaces and metamaterials (Xia *et al.*, 2017). Artificial metamaterials refer to an artificially synthesized class of materials with properties distinct from traditional materials without violating objective physical laws (Liu *et al.*, 2020a). Manipulating sound waves, such as acoustic cloaking (Popa *et al.*, 2011), acoustic emission (Landi *et al.*, 2018), acoustic negative refraction (García-Chocano *et al.*, 2014; He *et al.*, 2018), subwavelength imaging (Melde *et al.*, 2016; Tian *et al.*, 2017), wave-front modulation (Quan *et al.*, 2014; Xia *et al.*, 2017), and topological acoustics (Chen *et al.*, 2018; Quan *et al.*, 2018), has significant developments in artificial acoustic metamaterials with exotic efficient parameters. Conventional absorbing materials as materials containing porous require absorber material characterized as being thick when dealing with range having low-frequencies (Zhang *et al.*, 2018a). Different types of resonant elements may show different abnormal responses based on localized resonances. That can be referred to as physical parameters of negative components. Acoustic membranes (Huang *et al.*, 2018; Li, Assouar, 2016; Yang, Sheng, 2017) and rubber-coated rigid spheres (Yang *et al.*, 2017) are examples of dipolar resonance (Zhang *et al.*, 2018b) components that can yield negative effective mass density. Other monopolar resonance components such as Helmholtz resonators show the negative efficient bulk modulus (Shao *et al.*, 2019). An exciting and challenging issue is sound absorption in deep subwavelength space, especially at low frequencies. In this respect, conventional techniques, for instance porous materials, micro-perforated plates, and wedges for sound absorption, have significant limitations. New ideas to achieve sound absorption in unusual ways have recently been provided by the rapid development of acoustic metamaterials, i.e. artificial acoustic materials with almost arbitrary mass density and modulus (Duan *et al.*, 2015).

Liu *et al.* (2000) first constructed a locally resonant metamaterial and achieved control of acoustic waves on

a subwavelength scale. Li and Chan (2004) designed double negative AMMs by introducing a periodic arrangement of Helmholtz resonators. Yang *et al.* (2008) proposed membrane metamaterials to enable control of low-frequency waves. Due to the friction in thin canals during the resonance, Wu *et al.* (2016) used the energy dissipation. This theory makes it possible to obtain an absorption of 88.9% for a single metamaterial layer (Wu *et al.*, 2018). Lee *et al.* (2019) indicated arrays of coupled Helmholtz resonators with more than 90% absorption at 2200 Hz that could be used to adjust the direction of airflow at the same time. A stackable, ultra-open metamaterial absorber with broadband performance was designed by Xiang *et al.* (2019) with a calculation absorption coefficient above 0.6 in this 500 to 720 Hz frequency spectrum. However, these locally resonant metamaterials can only control waves at their resonant frequency, which causes high losses and leads to narrow operating bandwidths. Furthermore, to achieve the double negative property in locally resonant metamaterials, it is necessary to combine structures with a negative mass density and a negative bulk modulus, which causes construction difficulties and poor structural robustness, thus limiting the engineering application of these materials (Liu *et al.*, 2020b). Those metamaterials show extraordinary acoustic characteristics such as tuneable band (Lu *et al.*, 2015a; 2015b; 2016; 2017; Shrestha *et al.*, 2018; Yu *et al.*, 2017a, 2017b; 2017c), acoustic trapping, negative modulus, bandgap and effective negative mass (Lu *et al.*, 2020). Although little research has been done on this, acoustic metamaterial absorbers with near-zero modulus have been used for PA at a deep subwavelength scale.

The present work proposes perfect absorption systems using modulus-near-zero metamaterials in air or water with metamaterial I, II, and III, used to analyse the optimized sound isolation design and the perfect absorber. The energy dissipation due to friction in narrow channels during the resonance can be seen when comparing structures. The finite element simulations solver COMSOL Multiphysics software was utilized to search structural-acoustic interaction. Total sound absorption could be achieved at an extremely low frequency due to visco-thermal loss in the sub-wavelength slit of an acoustic metamaterial. It is possible to adjust the dissipation loss to achieve the perfect absorption condition by adjusting the width of the metamaterial structure's slit.

Contrary to the work conducted previously by Shao *et al.* (2019), which focused on PA by deducting analytically and demonstrating numerically that the MA with a suitable imaginary part and a vanishing real part of the bulk modulus can acquire perfect absorber, in this paper we develop a general theory to get PA with the modulus-near-zero (MNZ) metamaterial immersed in air or underwater. Depending upon theoretical analysis, an acoustic metamaterial (AMMs) that supports resonance with a monopole is developed to construct a low-frequency sound-absorbing technology and is also a good candidate for low-frequency perfect sound absorbers.

2. Materials and methods

Recently, AMMs were developed for sound insulation at low frequencies (Chen *et al.*, 2014; Huang *et al.*, 2009; Lee *et al.*, 2009; Mei *et al.*, 2012; Naify *et al.*, 2011a; Shanshan *et al.*, 2008; Yang *et al.*, 2010). According to the local resonance mechanism, AMM can achieve total reflection and serve as a sound insulation material. For example, the membrane-type metamaterial is a typical sound insulation material. Comparing with sound insulation materials in nature, they have the capability of strong acoustic mitigation in a deep-subwavelength scale (Ma *et al.*, 2015; Ma *et al.*, 2014; Naify *et al.*, 2011b; Xiao *et al.*, 2015; Yang *et al.*, 2013; 2015). Sound insulation of noise is appropriate and better by using such material to evaluate sound insulation properties of complex materials. The structure of the theoretical model consisting of air or underwater acoustic metamaterial and rubber material with realistic geometric thickness d is shown in Fig. 1a and is denoted as regions 1, 0,

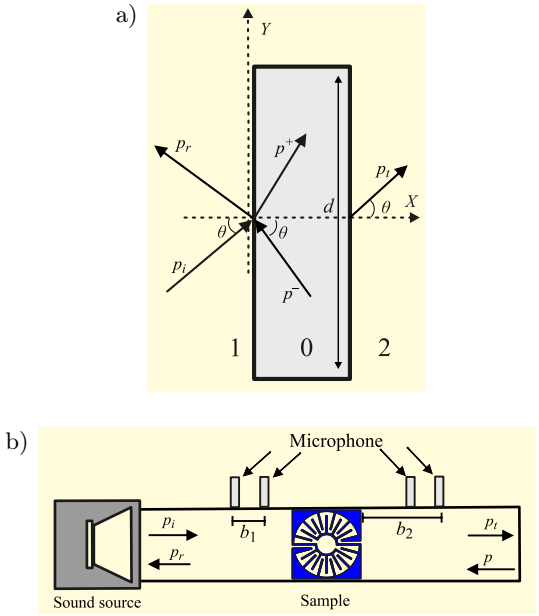

Fig. 1. a) Schematic diagram, the metamaterial slab (region 0) is located between two regions (1, 2) where d (geometric thickness) and p_i, p_r, p_o^-, p_o^+, and p_t are the pressure field amplitudes in the region 1, region 0, and region 2, respectively; b) the samples (metamaterial slab) were placed between two aluminum tubes with square cross-sections, four microphones in the two-port technique, where p_i, p_r, p_t, p are the complex amplitudes of the incident, reflected and transmitted plane waves, respectively.

and 2, respectively. The air density is 1.21 kg/m^3, the water density is 1000 kg/m^3, and the rubber density is 1300 kg/m^3, while the corresponding bulk modulus of the air is $1.42 \cdot 10^5$ N/m^2, the water is $2.22 \cdot 10^9$ N/m^2 and the rubber is $2.6 \cdot 10^8$ N/m^2. The metamaterials were placed in an aluminium tube with a square cross-section, as presented in Fig. 1b. It is thus possible to write the complex form of the time-harmonic solution of sound wave pressure as (Mahjoob *et al.*, 2009)

$$p_n = e^{-i\omega t}\left[p_n^+ e^{-ikx} + p_n^- e^{ikx}\right]. \tag{1}$$

The equations of the sound wave in the region (1), (0), and (2) in Fig. 1a are as follows:

$$p_1 = e^{-i\omega t}\left[p_i e^{ik(x\cos\theta + y\sin\theta)} + p_r e^{ik(x\cos\theta - y\sin\theta)}\right], \tag{2}$$

$$p_o = e^{i\omega t}\left[p_o^+ e^{-ik_o(x\cos\theta_o + y\sin\theta_o)} + p_o^- e^{ik_o(x\cos\theta_o - y\sin\theta_o)}\right], \tag{3}$$

$$p_2 = e^{i\omega t}\left[p_t e^{-ik(x\cos\theta + y\sin\theta)}\right], \tag{4}$$

where p_n^+ and p_n^- are the pressure field amplitudes in the region n ($n = 0, 1$, and 2), w is the angular frequency, k is the effective wave number for sound waves propagating inside the structure ($k = 2\pi f/c$), where f indicates the frequency in Hz, and c sound velocity of the air is 343 m/s, t is time, and θ is the incident angle of sound waves. The complex pressures at the measurement positions are then (Feng, 2013):

$$p_1^- = p_i\, e^{ika_1} + p_r\, e^{-ika_1}, \tag{5}$$

$$p_1^+ = p_i\, e^{ika_2} + p_r\, e^{-ika_2}, \tag{6}$$

$$p_2^- = p\, e^{ika_3} + p_t\, e^{-ika_3}, \tag{7}$$

$$p_2^+ = p\, e^{ika_4} + p_t\, e^{-ika_4}, \tag{8}$$

where p_t, p_r, and p_i are transmitted, reflected, and incident plane modes (Feng, 2013). From previous equations, the reflection, transmission and absorption coefficients are obtained as follows:

$$R = \frac{p_r}{p_i} = \frac{[p_1^+ - p_1^- \exp(-ikb_1)]\exp(ikb_2)}{[p_1^- \exp(-ikb_1) - p_1^+]\exp(-ikb_2)}, \tag{9}$$

$$T = \frac{p_t}{p_i} = \frac{[p_2^- - p_2^+ \exp(-ikb_1)]\exp(ikb_2)}{[p_1^- \exp(-ikb_1) - p_1^+]\exp(-ikb_2)} \tag{10}$$

$$\alpha = 1 - |R|^2 - |T|^2. \tag{11}$$

In formula $b_1 = a_1 - a_2 = a_4 - a_3$ and $b_2 = a_1 = a_4$ since the microphones are symmetrically placed about the metamaterial slab, where p_1^-, p_1^+, p_2^-, and p_2^+ are the pressure field amplitudes, respectively.

3. Results and discussions

3.1. The metamaterial (I) in air or underwater

The acoustic metamaterial that absorbs the largest possible amount of sound waves reflects the least possible of them, and at the same time, transmits more waves. The sound travels in the form of waves that can be absorbed by structures or reflected on them, and the best types of structures to absorb sounds are those that have rough surfaces, holes, or zigzag inside them. The appropriate structure picks up the sound waves and moves them inside so fewer vibrations produce the perfect absorption. Figure 2 shows the absorption coefficient of acoustic metamaterial (I) in air or underwater at a frequency range of 100–1000 Hz. The absorption does not appear in one and two structures but is only achieved in a four-structure with a slit width of 2.5 mm, as shown in Fig. 2a. In the air, the absorption peak with coefficients 0.34 and 0.36 appears at 310 Hz and 690 Hz (Fig. 2b). In Fig. 2c, absorption coefficients

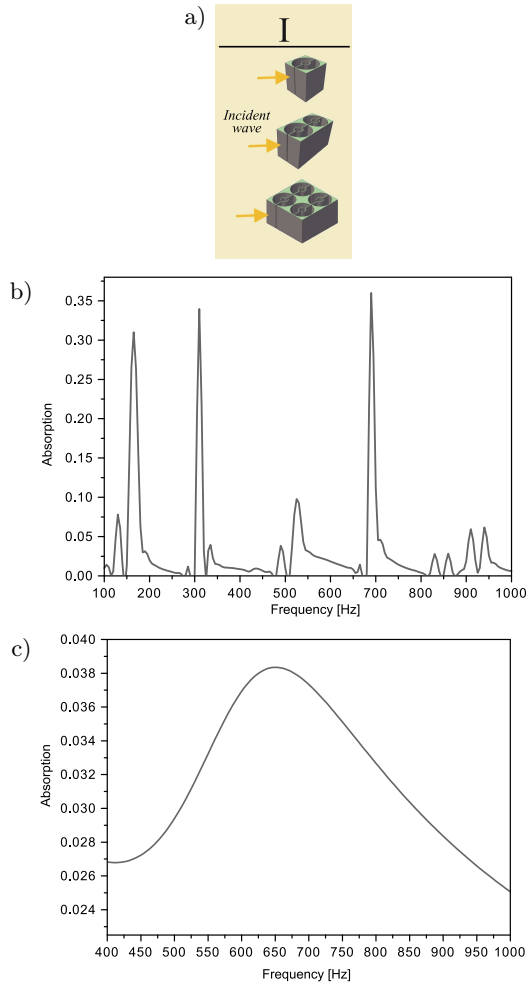

Fig. 2. a) Schematic arrangement of metamaterial I in one, two, and four structures, respectively, at slit width (2.5 mm). The absorption coefficients for metamaterial I (four-structure) as a function of frequency (b) in the air (c) underwater.

are slightly less than 0.1 within the range from 100–1000 Hz underwater. The incident waves pass through this structure, and the non-trapped energy in the resonant element produces a large rate from reflection and transmission coefficients.

3.2. Comparison between metamaterial (II) and metamaterial (III) in air

In order to create a perfect absorber, we built the metamaterial structure to fulfil the perfect absorber (PA) condition. The cross-sectional schematic view of the metamaterial structure, indicating zero mass density and bulk modulus, is shown in Fig. 3a. The metamaterials' outer and inner radii are R_1 and R_2, respectively. The structure is uniformly divided into two parts. Each portion has an interdigital zigzag channel with the outer slit width w_1, the inner slit width w_2, and the wall thickness t; slit width w showing a partition chart of modulus-near-zero acoustic metamaterials geometric parameters is shown in Table 1. This chart focuses on the metamaterial II and III in air, referring to the highlighted domains in Fig. 3b. Searching for the incident sound waves entering through to slit width in metamaterial II and III paves the way to achieve the PA. In metamaterial III, we used the incident sound waves to enter one side onto a homogenous metamaterial slab with a changed slit width of 2.5 mm. We employed the equations to calculate the optimum sound absorption. We started the analysis by conducting metamaterial II, III (one, two, and four structures) and determining the perfect absorption at low frequencies, as shown in Fig. 4. At resonance frequencies of 280 Hz and 120 Hz, we show a high peak of perfect absorption at 0.79 and 0.99, respectively, in one-structure metamaterial slab II and III in Fig. 4a.

The absorption spectrum is shown in Figs 4b and 4c, where two-structure and four-structure data are well-matched in metamaterial slab II, and III, and are marked in Fig. 3b. Figure 4b shows the measured acoustic absorber at 0.89 and 0.95 in the frequency ranges at 145 Hz and 270 Hz, respectively. From Fig. 4c, unitary sound absorption occurs at 140 Hz and 260 Hz. These results demonstrate that the

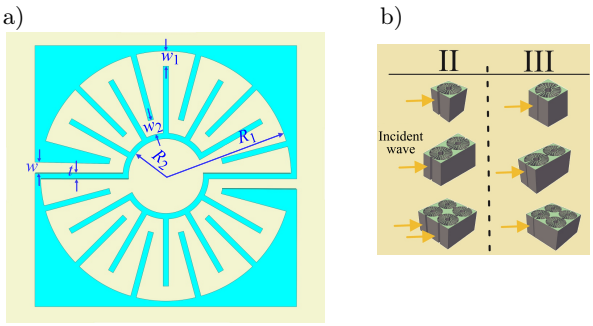

Fig. 3. a) Designed metamaterial units, b) The schematic diagram for the left-side metamaterial slab II at slit width (7.8 mm) and the right-side of the incident sound waves to enter one side onto homogenous metamaterial slab III at a slit width (2.5 mm).

Table 1. Geometric parameters of the modulus-near-zero metamaterial slab.

Slab	R_1 [mm]	R_2 [mm]	w_1 [mm]	w_2 [mm]	w [mm]	t [mm]	d [mm] one-structure	d [mm] four-structure
II	33.5	10	4	4	7.8	1.5	70	140
III	33.5	10	4	4	2.5	1.5	70	140

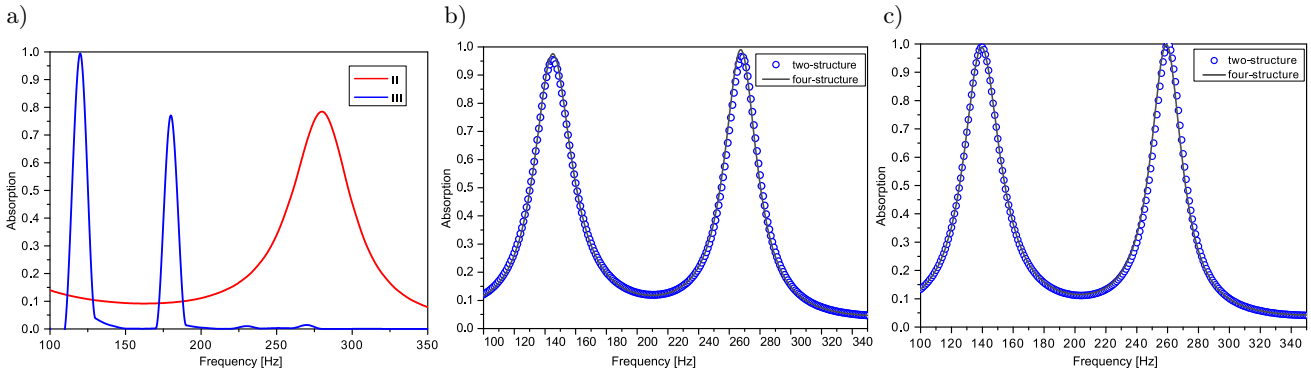

Fig. 4. Absorption coefficients as frequency function for: a) one-structure in metamaterial slab II and III, b) two and four-structure in metamaterial slab II, c) two and four-structure in metamaterial slab III in air.

metamaterial slab III sound absorption peak is slightly higher than metamaterial II. It is found that the transmission and reflection coefficients are almost cancelled (~0) for quantifying the optimum amount of absorbed energy in this structure via adjusting the slit width and the visco-thermal effect of controlling the loss of the metamaterial acoustic. Consequently, the slit width plays a part in suppressing the transmission and decreases the reflection because of destructive interference. These results indicate that the newly designed metamaterial III has excellent absorber acoustic properties and will be promising in engineering applications.

3.3. Comparison between metamaterial (II) and metamaterial (III) in underwater

The impedance matching with the background is one of the most important things for interacting a resonant loss structure with an incoming wave. We characterized both the intrinsic loss and the leakage rate of energy at the resonant frequency. The balance between the loss and the leakage generates a maximum energy absorption, corresponding to the critical coupling condition that traps the energy around resonance elements. The energy trapped in the resonance element was used to perfectly absorb the energy, i.e. without transmission or reflection in transmission systems. For the simulation demonstration of the perfect absorption onto acoustic metamaterial, we modelled a composite material of the metamaterial slab II and III underwater. In Fig. 5a, absorption coefficients show 0.562 and 0.205 at 311 Hz and 310 Hz, respectively, in one structure because PA differs from each other due to the different slit widths of the metamaterial. Figures 5b and 5c show the absorption coefficient of the metamaterial slab II and III underwater in two and four-structure, respectively. The results clearly show a perfect absorption peak in metamaterial slab II and III at around 338 Hz, and 340 Hz is 0.96 and 0.88, respectively, for two-structure and unitary sound absorbers at four-structure. However, the simulation results reveal that the MNZ (four-structure) underwater within the frequency range of 338 Hz and 340 Hz leads to an optimum absorption. The absorption peak is stimulated by intense underwater resonance in the width of the slit. Then the sound energy is essentially dissipated by viscous damping and loss of friction. As a result, the energy of the incidence wave is generally consumed because of the more considerable friction occurring between the slit width and acoustic wave. Hence, the absorption mechanism with a low-frequency range regarding an acoustic absorber converts the acoustic energy to thermal energy in the resonant frequency.

4. Conclusions

In summary, we constructed acoustic metamaterials immersed in air or water by creating a metamaterial slab I, II, and III. Therefore, metamaterial structures for satisfying the perfect absorber (PA) at low frequency are designed. We focus on the concept of (MNZ) metamaterials in acoustic waves, both air and underwater. A theory of the perfect absorber of modulus-near-zero metamaterials is proposed. The visco-thermal dissipation has a significant impact on the slow sound propagation in waveguides. This feature was exploited for low-frequency acoustic absorbers, which play an essential role in sound absorption in AMMs containing slits of subwavelength. Because of the existence of the loss technique, the behaviour at Fabry-Pérot resonances relies ideally upon the effective geometry permeability-near-zero material slab, slit width, and medium that could be detected for achieving higher absorption. At the frequency of resonance < 500 Hz, the effect of sound-absorbing materials possibly reaches 99%. The friction loss of sound wave energy contributes extremely to better performance regarding sound absorbing of this material.

Furthermore, the theory of the MNZ can be used to clarify the other cases' absorption in a way. The idea of designing the modulus-near-zero metamaterial acoustic can be propagated directly to the optimum sound absorption design in the path of propagation.

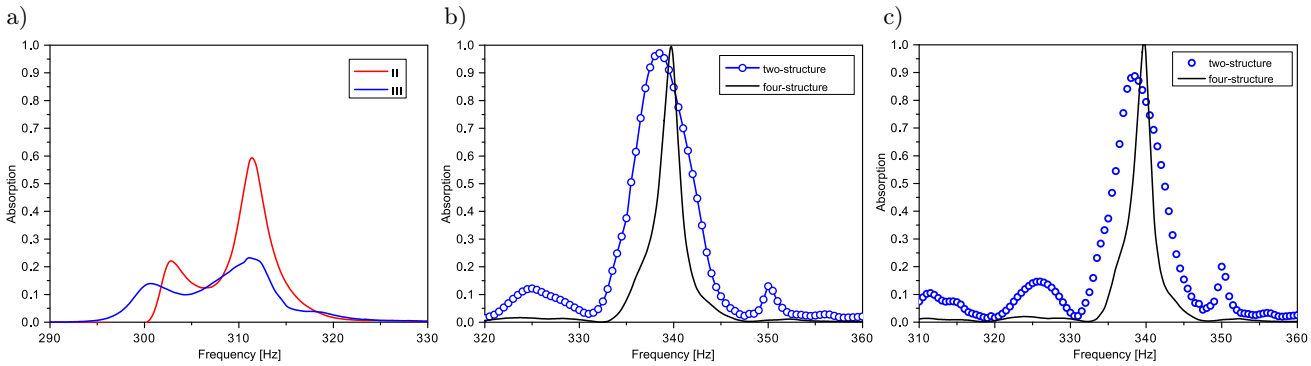

Fig. 5. Absorption coefficients as frequency function for: a) One-structure in metamaterial slab II and III, b) two and four-structure in metamaterial slab II, c) two and four-structure in metamaterial slab III in underwater.

Our design has a high sparsity advantage compared to previous metamaterials, ease of fabrication in 3D printing, and robustness in practical applications.

References

1. Chen J., Huang H., Huo S., Tan Z., Xie X., Cheng J. (2018), Self-ordering induces multiple topological transitions for elastic waves in phononic crystals, *Physical Review B*, **98**(1): 14302, doi: 10.1103/PhysRevB.98.014302.
2. Chen Y., Huang G., Zhou X., Hu G., Sun C.-T. (2014), Analytical coupled vibroacoustic modeling of membrane-type acoustic metamaterials: Plate model, *The Journal of the Acoustical Society of America*, **136**(6): 2926–2934, doi: 10.1121/1.4901706.
3. Duan Y. *et al.* (2015), Theoretical requirements for broadband perfect absorption of acoustic waves by ultra-thin elastic meta-films, *Scientific Reports*, **5**(1): 12139, doi: 10.1038/srep12139.
4. Feng L. (2013), Modified impedance tube measurements and energy dissipation inside absorptive materials, *Applied Acoustics*, **74**(12): 1480–1485, doi: 10.1016/j.apacoust.2013.06.013.
5. García-Chocano V.M., Christensen J., Sánchez-Dehesa J. (2014), Negative refraction and energy funneling by hyperbolic materials: An experimental demonstration in acoustics, *Physical Review Letters*, **112**(14): 144301, doi: 10.1103/PhysRevLett.112.144301.
6. He H. *et al.* (2018), Topological negative refraction of surface acoustic waves in a Weyl phononic crystal, *Nature*, **560**(7716), 61–64, doi: 10.1038/s41586-018-0367-9.
7. Huang H.H., Sun C.T., Huang G.L. (2009), On the negative effective mass density in acoustic metamaterials, *International Journal of Engineering Science*, **47**(4): 610–617, doi: 10.1016/j.ijengsci.2008.12.007.
8. Huang S., Fang X., Wang X., Assouar B., Cheng Q., Li Y. (2018), Acoustic perfect absorbers via spiral metasurfaces with embedded apertures, *Applied Physics Letters*, **113**(23): 233501, doi: 10.1063/1.5063289.
9. Landi M., Zhao J., Prather W.E., Wu Y., Zhang L. (2018), Acoustic purcell effect for enhanced emission, *Physical Review Letters*, **120**(11): 114301, doi: 10.1103/PhysRevLett.120.114301.
10. Lee S.H., Park C.M., Seo Y.M., Wang Z.G., Kim C.K. (2009), Acoustic metamaterial with negative density, *Physics Letters, Section A: General, Atomic and Solid State Physics*, **373**(48): 4464–4469, doi: 10.1016/j.physleta.2009.10.013.
11. Lee T., Nomura T., Dede E.M., Iizuka H. (2019), Ultrasparse acoustic absorbers enabling fluid flow and visible-light controls, *Physical Review Applied*, **11**(2): 24022, doi: 10.1103/PhysRevApplied.11.024022.
12. Li J., Chan C.T. (2004), Double-negative acoustic metamaterial, *Physical Review E – Statistical Physics, Plasmas, Fluids, and Related Interdisciplinary Topics*, **70**(5): 4, doi: 10.1103/PhysRevE.70.055602.
13. Li Y., Assouar B.M. (2016), Acoustic metasurface-based perfect absorber with deep subwavelength thickness, *Applied Physics Letters*, **108**(6): 63502, doi: 10.1063/1.4941338.
14. Liu J., Guo H., Wang T. (2020a), A review of acoustic metamaterials and phononic crystals, *Crystals*, **10**(4): 305, doi: 10.3390/cryst10040305.
15. Liu Y. *et al.* (2020b), Three-dimensional fractal structure with double negative and density-near-zero properties on a subwavelength scale, *Materials and Design*, **188**: 108470, doi: 10.1016/j.matdes.2020.108470.
16. Liu Z. *et al.* (2000), Locally resonant sonic materials, *Science*, **289**(5485): 1734–1736, doi: 10.1126/science.289.5485.1734.
17. Lu Z., Cui Y., Debiasi M. (2016), Active membrane-based silencer and its acoustic characteristics, *Applied Acoustics*, **111**: 39–48, doi: 10.1016/j.apacoust.2016.03.042.
18. Lu Z., Cui Y., Debiasi M., Zhao Z. (2015a), A tunable dielectric elastomer acoustic absorber, *Acta Acustica United with Acustica*, **101**(4): 863–866, doi: 10.3813/ AAA.918881.
19. Lu Z., Godaba H., Cui Y., Foo C.C., Debiasi M., Zhu J. (2015b), An electronically tunable duct silencer using dielectric elastomer actuators, *The Journal of the Acoustical Society of America*, **138**(3): EL236–EL241, doi: 10.1121/1.4929629.
20. Lu Z., Shrestha M., Lau G.K. (2017), Electrically tunable and broader-band sound absorption by using micro-perforated dielectric elastomer actuator, *Applied Physics Letters*, **110**(18), 182901, doi: 10.1063/1.4982634.
21. Lu Z., Yu X., Lau S.K., Khoo B.C., Cui F. (2020), Membrane-type acoustic metamaterial with eccentric masses for broadband sound isolation, *Applied Acoustics*, **157**: 107003, doi: 10.1016/j.apacoust.2019.107003.
22. Ma F., Wu J.H., Huang M. (2015), Resonant modal group theory of membrane-type acoustical metamaterials for low-frequency sound attenuation, *EPJ Applied Physics*, **71**(3): 30504, doi: 10.1051/epjap/2015150310.
23. Ma G., Yang M., Xiao S., Yang Z., Sheng P. (2014), Acoustic metasurface with hybrid resonances, *Nature Materials*, **13**(9): 873–878, doi: 10.1038/nmat3994.
24. Mahjoob M.J., Mohammadi N., Malakooti S. (2009), An investigation into the acoustic insulation of triple-layered panels containing Newtonian fluids: theory and experiment, *Applied Acoustics*, **70**(1): 165–171, doi: 10.1016/j.apacoust.2007.12.002.
25. Mei J., Ma G., Yang M., Yang Z., Wen W., Sheng P. (2012), Dark acoustic metamaterials as super absorbers for low-frequency sound, *Nature Communications*, **3**(1): 1–7, doi: 10.1038/ncomms1758.

26. Melde K., Mark A.G., Qiu T., Fischer P. (2016), Holograms for acoustics, *Nature*, **537**(7621): 518–522, doi: 10.1038/nature19755.

27. Naify C.J., Chang C.-M., McKnight G., Nutt S. (2011a), Transmission loss of membrane-type acoustic metamaterials with coaxial ring masses, *Journal of Applied Physics*, **110**(12): 124903, doi: 10.1063/1.3665213.

28. Naify C.J., Chang C.-M., McKnight G., Scheulen F., Nutt S. (2011b), Membrane-type metamaterials: Transmission loss of multi-celled arrays, *Journal of Applied Physics*, **109**(10): 104902, doi: 10.1063/1.3583656.

29. Popa B.I., Zigoneanu L., Cummer S.A. (2011), Experimental acoustic ground cloak in air, *Physical Review Letters*, **106**(25): 253901, doi: 10.1103/PhysRevnLett.106.253901.

30. Quan L., Ra'di Y., Sounas D., Alů A. (2018), Maximum Willis coupling in acoustic scatterers, *Physical Review Letters*, **120**(25): 254301, doi: 10.1103/PhysRevLett.120.254301.

31. Quan L., Zhong X., Liu X., Gong X., Johnson P.A. (2014), Effective impedance boundary optimization and its contribution to dipole radiation and radiation pattern control, *Nature Communications*, **5**(1): 1–8, doi: 10.1038/ncomms4188.

32. Shanshan Y., Xiaoming Z., Gengkai H. (2008), Experimental study on negative effective mass in a 1D mass-spring system, *New Journal of Physics*, **10**(4): 43020, doi: 10.1088/1367-2630/10/4/043020.

33. Shao C., Long H., Cheng Y., Liu X. (2019), Low-frequency perfect sound absorption achieved by a modulus-near-zero metamaterial, *Scientific Reports*, **9**(1): 1–8, doi: 10.1038/s41598-019-49982-5.

34. Shrestha M., Lu Z., Lau G.K. (2018), Transparent tunable acoustic absorber membrane using inkjet-printed PEDOT:PSS thin-film compliant electrodes, *ACS Applied Materials and Interfaces*, **10**(46): 39942–39951, doi: 10.1021/acsami.8b12368.

35. Tian Y., Wei Q., Cheng Y., Liu X. (2017), Acoustic holography based on composite metasurface with decoupled modulation of phase and amplitude, *Applied Physics Letters*, **110**(19): 191901, doi: 10.1063/1.4983282.

36. Wu X. *et al.* (2016), Low-frequency tunable acoustic absorber based on split tube resonators, *Applied Physics Letters*, **109**(4): 43501, doi: 10.1063/1.4959959.

37. Wu X. *et al.* (2018), High-efficiency ventilated metamaterial absorber at low frequency, *Applied Physics Letters*, **112**(10): 103505, doi: 10.1063/1.5025114.

38. Xia J.P., Sun H.X., Yuan S.Q. (2017), Modulating sound with acoustic metafiber bundles, *Scientific Reports*, **7**(1): 8151, doi: 10.1038/s41598-017-07232-6.

39. Xiang X. *et al.* (2019), Ultra-open high-efficiency ventilated metamaterial absorbers with customized broadband performance, *Applied Physics Letters*, **112**(10): 103505, doi: 10.1063/1.5025114.

40. Xiao S., Ma G., Li Y., Yang Z., Sheng P. (2015), Active control of membrane-type acoustic metamaterial by electric field, *Applied Physics Letters*, **106**(9): 91904, doi: 10.1063/1.4913999.

41. Yang M., Chen S., Fu C., Sheng P. (2017), Optimal sound-absorbing structures, *Materials Horizons*, **4**(4): 673–680, doi: 10.1039/C7MH00129K.

42. Yang M. *et al.* (2015), Sound absorption by subwavelength membrane structures: A geometric perspective, *Comptes Rendus – Mecanique*, **343**(12): 635–644, doi: 10.1016/j.crme.2015.06.008.

43. Yang M., Ma G., Yang Z., Sheng P. (2013), Coupled membranes with doubly negative mass density and bulk modulus, *Physical Review Letters*, **110**(13): 134301, doi: 10.1103/PhysRevLett.110.134301.

44. Yang M., Sheng P. (2017), Sound absorption structures: from porous media to acoustic metamaterials, *Annual Review of Materials Research*, **47**: 83–114, doi: 10.1146/annurev-matsci-070616-124032.

45. Yang Z., Dai H.M., Chan N.H., Ma G.C., Sheng P. (2010), Acoustic metamaterial panels for sound attenuation in the 50–1000 Hz regime, *Applied Physics Letters*, **96**(4): 041906, doi: 10.1063/1.3299007.

46. Yang Z., Mei J., Yang M., Chan N.H., Sheng P. (2008), Membrane-type acoustic metamaterial with negative dynamic mass, *Physical Review Letters*, **101**(20): 204301, doi: 10.1103/PhysRevLett.101.204301.

47. Yu X., Lu Z., Cheng L., Cui F. (2017a), On the sound insulation of acoustic metasurface using a substructuring approach, *Journal of Sound and Vibration*, **401**: 190–203, doi: 10.1016/j.jsv.2017.04.042.

48. Yu X., Lu Z., Cheng L., Cui F. (2017b), Vibroacoustic modeling of an acoustic resonator tuned by dielectric elastomer membrane with voltage control, *Journal of Sound and Vibration*, **387**: 114–126, doi: 10.1016/j.jsv.2016.10.022.

49. Yu X., Lu Z., Cui F., Cheng L., Cui Y. (2017c), Tunable acoustic metamaterial with an array of resonators actuated by dielectric elastomer, *Extreme Mechanics Letters*, **12**: 37–40, doi: 10.1016/j.eml.2016.07.003.

50. Zhang Z., Cheng Y., Liu X. (2018a), Achieving acoustic topological valley-Hall states by modulating the subwavelength honeycomb lattice, *Scientific Reports*, **8**(1): 16784, doi: 10.1038/s41598-018-35214-9.

51. Zhang Z. *et al.* (2018b), Directional acoustic antennas based on Valley-Hall topological insulators, *Advanced Materials*, **30**(36): 1803229, doi: 10.1002/adma.201803229.